

# Forest Inventory Assessment Using Integrated Light Detection and Ranging (LiDAR) Systems: Merged Point Cloud of Airborne and Mobile Laser Scanning Systems

Yongkyu Lee,<sup>1†</sup> Heesung Woo,<sup>2†</sup> and Jung-Soo Lee<sup>1\*</sup>

<sup>1</sup>Department of Forest Management, Kangwon National University, Chuncheon 24341, Republic of Korea

<sup>2</sup>College of Forest and Environmental Sciences, Kangwon National University,  
Chuncheon 24341, Republic of Korea

(Received September 8, 2022; accepted December 12, 2022)

**Keywords:** airborne laser scanning (ALS), mobile laser scanning (MLS), precision forestry, forest inventory, remote sensing

Precise assessment of forest inventory can help optimize timber value and industrial forest-management planning. Light detection and ranging (LiDAR) technology has been recently introduced in forestry to effectively and precisely estimate and monitor forest inventories. In this study, we investigated the opportunities and limitations of integrated mobile laser scanning (MLS) and airborne laser scanning (ALS) LiDAR applications for estimating individual tree diameter at breast height (DBH) and tree height. Three circular fitting algorithms (integrated RANSAC and circle fitting, minimum enclosing circle, and least-squares ellipse fitting) were used to estimate DBH. Height was calculated using the crown height model (CHM). DBH was most accurately estimated by the ellipse-fitting algorithm. Integrated MLS and ALS performed better than previous circular fitting applications in estimating DBH values. Lastly, the tree height estimated using the CHM was compared with the ground truth, and  $R^2$  and the root mean square error (RMSE) of the height were 0.60 and 2.0 m, respectively. In addition, the trend of low accuracy for suppressed trees was identified from point cloud data (PCD) extraction because of overlapped PCD among the surrounding dominant trees. This result indicated that the segmentation of the top of suppressed trees was limited by overlap issues in high-density forests.

## 1. Introduction

Accurate forest inventory assessment is crucial in the forest industry. The composition, structure, and estimated volume of forests are essential information in the forest industry for optimizing timber value and for effective forest-management planning.<sup>(1)</sup> Forest inventory assessment through the collection of the diameter at breast height (DBH), tree height, and tree location data requires field-based methods. However, traditional forest inventory assessment methods have key limitations, such as high labor costs, excessive time consumption, and suboptimal data continuity. Additionally, access to dangerous areas, including remote areas and

---

\*Corresponding author: e-mail: [jslee72@kangwon.ac.kr](mailto:jslee72@kangwon.ac.kr)

†These authors contributed equally to this work.

<https://doi.org/10.18494/SAM4100>

steep terrain, is limited.<sup>(2)</sup> To overcome these limitations, several groups have investigated efficient ways to obtain forest inventory data using remote sensing techniques.<sup>(3)</sup>

Remotely sensed data, satellite images, sensor-collected data, and light detection and ranging (LiDAR) applications are widely used for assessing forest inventory. LiDAR applications have recently been introduced as an effective tool for precisely estimating and monitoring forest inventories.<sup>(3)</sup> Several studies have been conducted using LiDAR sensors in forestry, including those for forest biomass estimation, forest canopy height assessment, and tree volume estimation.<sup>(4–6)</sup> Various types of forest data have been estimated using LiDAR systems. However, tree diameter measurement is the most common use of LiDAR systems. In LiDAR systems for forest applications, three types of scanning systems—airborne laser scanning (ALS), terrestrial laser scanning (TLS), and mobile laser scanning (MLS) systems—are commonly used for 3D mapping. ALS is commonly used in large areas. However, the capture of under-canopy point data is limited. TLS is the most accurate method for collecting 3D point clouds in forestry, but there are still barriers to capturing surrounding point data in the forest area. To overcome the limitations of ALS and TLS, MLS is used as an alternative tool for rapidly assessing and monitoring forest inventory. MLS helps prevent an increase in the rates of occlusion and missing data in high-density forests.<sup>(7)</sup> Liu *et al.* estimated the height and DBH of individual trees using MLS point cloud data (PCD) and obtained a root mean square error (RMSE) of 3.17 cm for DBH in a natural forest plot.<sup>(8)</sup> Woo *et al.* also investigated individual tree diameters using four circular fitting algorithms. They found that the least-squares circle and minimum-enclosing circle algorithms were the most accurate for estimating tree diameter in *Pinus densiflora* and *Pinus koraiensis* forest stands.<sup>(9)</sup> Recently, unmanned aerial vehicles (UAVs) equipped with LiDAR systems for ALS have been widely adopted in large-scale forests. ALS allows scanning over a large area and is increasingly being used to determine forest canopy structures.<sup>(10)</sup> However, ALS has limitations in collecting under-canopy PCD data compared with MLS.<sup>(7)</sup> To overcome the limitations of MLS and ALS, several attempts have been made to merge MLS and ALS PCD to improve the accuracy of under-canopy PCD. Currently, the potential of combining the MLS and ALS systems for directly measuring forest structure parameters in forest inventory assessment remains underexplored.<sup>(11)</sup>

Unfortunately, the application of LiDAR sensors remains limited in forestry, a small-scale industry, in South Korea, because of the high cost of sensors and lack of information on LiDAR applications in forestry.<sup>(9)</sup> Hence, we investigated the opportunities and limitations of using the LiDAR technology to estimate the DBH and height of individual trees in South Korean forests.

## 2. Materials and Methods

The overall research process is illustrated in Fig. 1. PCD was collected using ALS and MLS. The collected PCD was boresighted and georeferenced using a post-processed kinematic (PPK) method. Three circular fitting algorithms were applied to the processed LiDAR PCD to estimate tree DBH. In addition, tree heights were calculated using the crown height model (CHM) with a 5 cm resolution. The CHM was generated on the basis of differences between the digital surface model (DSM) and the digital terrain model (DTM). Finally, the results of DBH and tree height

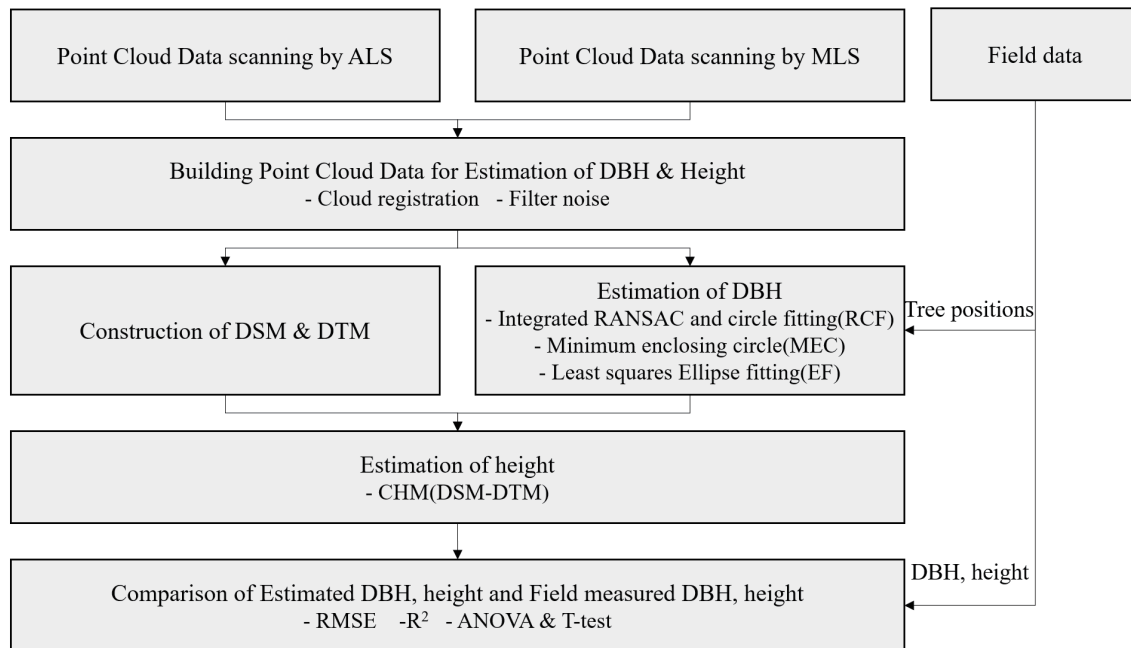


Fig. 1. Flowchart of overall research for estimating tree height and DBH.

estimations were validated by comparison with field-based ground truth data. The research process is described in detail in Fig. 1.

## 2.1 Site description

The study was conducted within the research forest of Kangwon National University, Hongcheon-gun, South Korea (Fig. 2). The research plot was a planted area dominated by *Pinus koraiensis*. The research plot was characterized by an even-aged plantation forest, and *Pinus koraiensis* was selected as the research target species. Fixed-radius plots were used for field data collection. In the sampling plot, an 11.3 m radius was measured from the center of the plot to the surrounding trees.

## 2.2 Field survey for DBH and tree height

Tree DBH (measured 1.2 m above ground level) was measured at the research site to validate the LiDAR DBH estimation. DBH of individual trees was measured using DBH tape. The mean value of the measured DBH was estimated as a representative value to validate the LiDAR DBH estimations. Tree height was measured using a Vertex 5 hypsometer and the height of each target tree was measured multiple times until the measured values were fixed. The total number of trees in each plot is 25. The average DBH in the field survey was 27.7 cm and the average tree height was 21.0 m.

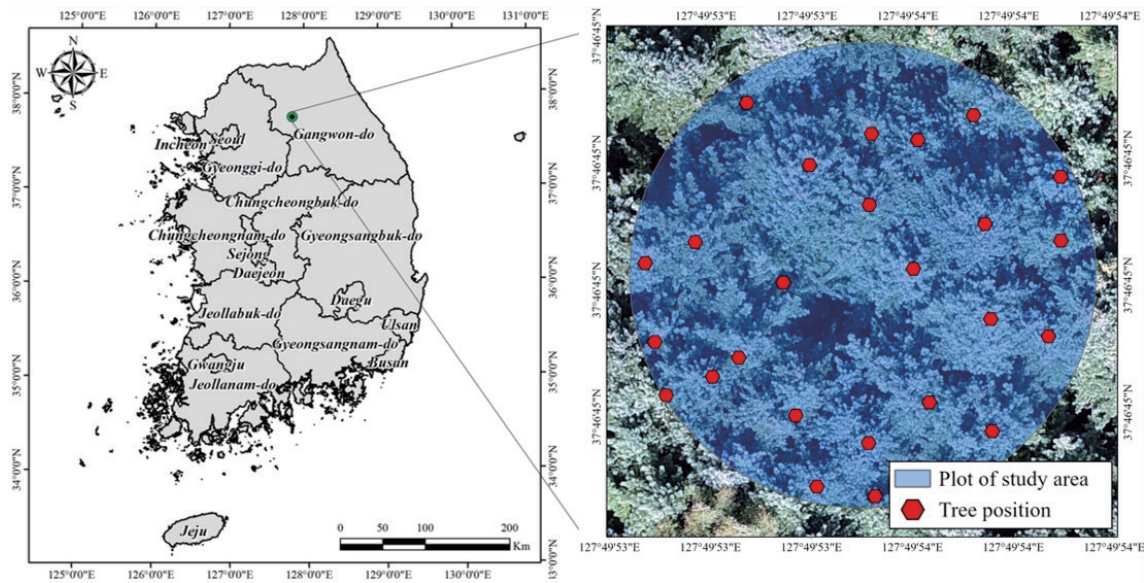


Fig. 2. (Color online) Research location and top view of the study area.

### 2.3 Point data collection using MLS

Mobile LiDAR data were collected on June 22, 2021 using a GeoSLAM Horizon laser scanning system (GeoSLAM Ltd., Nottinghamshire, UK) equipped with an inertial measurement unit (IMU) (Fig. 3). This system included a VLP-16 LiDAR sensor (Velodyne LiDAR, San Jose, CA, USA) equipped with a rotating motor to extend the field of view (FOV). The VLP-16 sensor generates a 903 nm wavelength, the angular step size is 0.1 to 0.4, and it has a beam divergence of 3 mrad. Various sensors and computer systems are attached to the GeoSLAM Horizon system, including the IMU, data storage, and power supply.<sup>(12)</sup> The collected LiDAR data were post-processed using the GeoSLAM HUB software to convert the PCD. The PCD was georeferenced in the Korea 2000 Korea Central Belt 2010 coordinate system using LiGeoreference 1.3.0 software (GreenValley International, Beijing, China).

### 2.4 Point data collection using ALS

ALS data were collected on June 22, 2021, using a DJI Matrice M300 RTK UAV (Da-Jiang Innovations Science and Technology Co. Ltd., China). This UAV, shown in Fig. 3, has a mass of 6.3 kg and four rotary wings, and can be operated at altitudes of up to 5000 m.<sup>(13)</sup> However, the allowed maximum altitude is set to 500 m in South Korea. The maximum flight time was limited to 55 min and the machine was equipped with an anticollision system. In this research, the GeoSLAM Horizon LiDAR system was mounted on the UAV to collect aerial LiDAR PCD. ALS LiDAR data were collected during a 20 min flight at an altitude of 50 m with a flight speed of 3 m/s.<sup>(11)</sup> The collected LiDAR PCD are based on a PPK flight trajectory produced using the Trimble r12i (Trimble, USA) GNSS base station.<sup>(14)</sup>



Fig. 3. (Color online) GeoSLAM sensor mounted on a backpack and M300 RTK. (a) MLS. (b) ALS.

## 2.5 Merging MLS and ALS point cloud data

The iterative closest point (ICP) algorithm was adopted to reduce the errors between the two sets of PCD. Errors occurred from autonomous matching using a statistical procedure or manual PCD matching process.<sup>(15)</sup> The ICP algorithm is expressed as

$$E(R, t) = \min_{R, t} \sum_i a_i - (Rq_i + -t)^2, \quad (1)$$

where  $p_i \in P$  is a point from the 3D reference PCD, and  $q_i \in Q$  is a point from the target PCD.

## 2.6 DBH and tree height estimation

Individual tree PCD were segmented on the basis of a field-survey map. The locations of individual trees were recorded during the field survey and a map of individual tree locations was used to segment the PCD of individual trees. The PCD of the DBH were automatically extracted at the breast height (1.2 m) using a digital elevation model (DEM). Extracted point clouds were used to estimate the DBH using circular fitting algorithms. The three circular fitting algorithms applied were integrated RANSAC and circle fitting (RCF), minimum enclosing circle (MEC), and least-squares ellipse fitting (EF).<sup>(16,17)</sup> The estimated DBHs were analyzed in Python 3.8.8, using NumPy and Matplotlib libraries [Fig. 4(a)]. In previous studies, the number of iterations used in the RANSAC algorithm to estimate the DBH of individual trees was set to 50, 200, and 1000.<sup>(16–18)</sup> However, the optimal number of iterations for investigating tree DBH has not been previously presented. We derived the optimal number of iterations by increasing the number of iterations at intervals of 10 from 10 to 90.

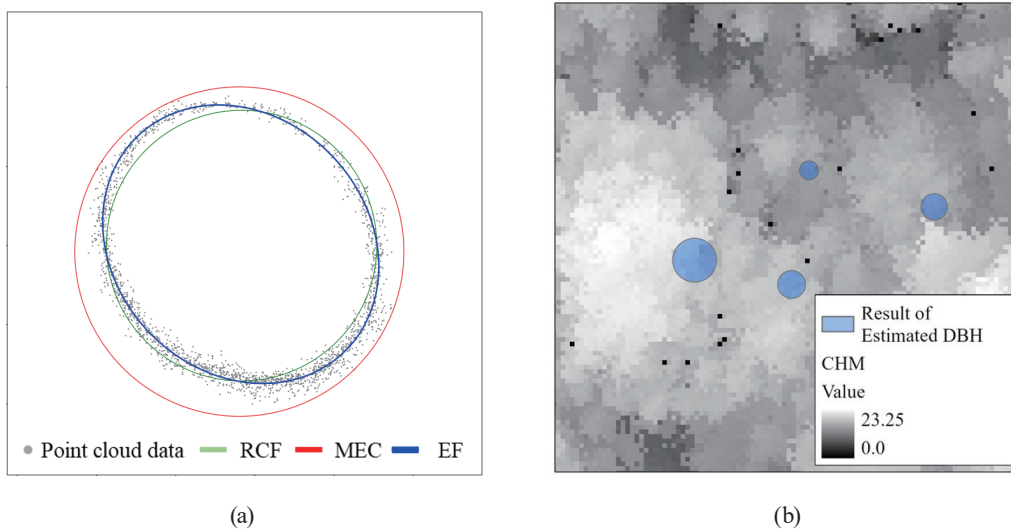


Fig. 4. (Color online) Examples of circular fitting outputs and tree height estimation. (a) Estimation of DBH. (b) Estimation of height.

To measure tree height, individual trees were divided into three categories based on the characteristics of PCD distribution patterns (Table 1). Tree height was estimated using the CHM with 5 cm resolution, where the CHM was based on the differences between the DSM and DTM [Fig. 4(b)].<sup>(19)</sup>

The estimated DBH and tree heights were validated using RMSE and bias. The coefficient of determination ( $R^2$ ) and RMSE equations are defined as

$$R^2 = \frac{\sum_{i=1}^n (\hat{y}_i - \bar{y})^2}{\sum_{i=1}^n (y_i - \bar{y})^2}, \quad (2)$$

$$\text{RMSE} = \sqrt{\frac{1}{n} \sum_{i=1}^n (y_i - \hat{y}_i)^2}, \quad (3)$$

where  $n$  is the number of estimates,  $\hat{y}_i$  is the estimated diameter at the  $i$ th tree, and  $y_i$  is the field-measured ground truth data.

### 3. Results and Discussion

#### 3.1 Point cloud data from LiDAR systems

A detailed description of the post-processed PCD is provided in Table 2. In total, 418813312 points were obtained from the study area. A permanent forest road was used to match two different PCD datasets (ALS and MLS). The numbers of forest road PCD captured by MLS and ALS were 30717544 and 764318, respectively. In the merging of the PCD, 7.5% of the MLS PCD

Table 1  
(Color online) Three defined PCD categories of the scanning results.

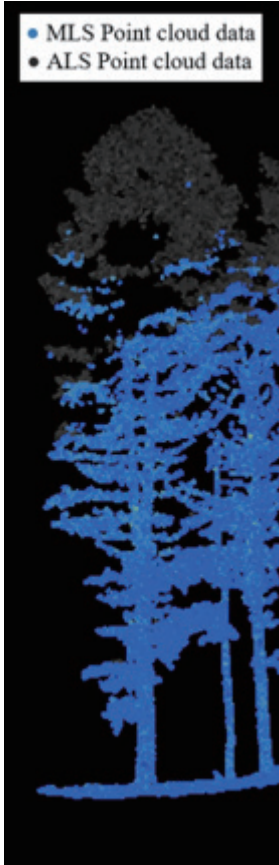
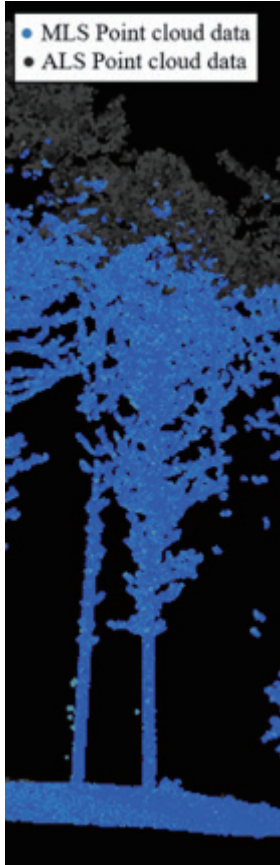
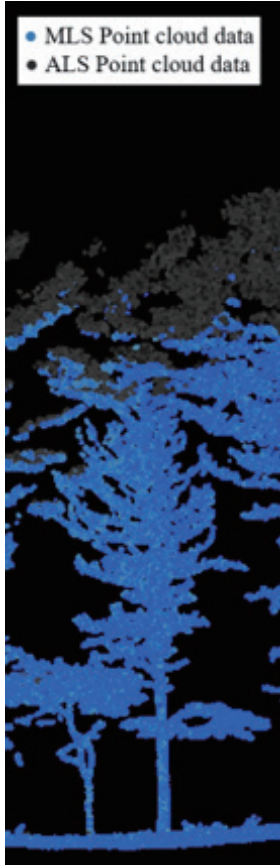
Types	A	B	C
Images			
Definitions	Type A: grows straight, unaffected by surrounding trees	Type B: can be affected by surrounding trees when measuring height owing to tilt	Type C: difficult to measure height using CHM as tree is suppressed

Table 2  
Detailed information on post-processed PCD.

Step	Process	Platform	Number of points
0	RAW	MLS	341101169
		ALS	77712143
1	Manual ICP matching	MLS	30717544
		ALS	764318
2	PCD after outlier removal	MLS	32625457
		ALS	544007
3	PCD after noise filtering	MLS	30005680
		ALS	504954
4	Merged PCD	ALL types	30510634

were used to apply the ICP algorithm. The RMSE of the ICP results was calculated to be 0.25 m. Statistical outlier removal (SOR) filtering was adopted in the noise removal process, and 2114823 points were removed. Finally, 30510634 PCD (7.2%) were used to estimate the individual tree

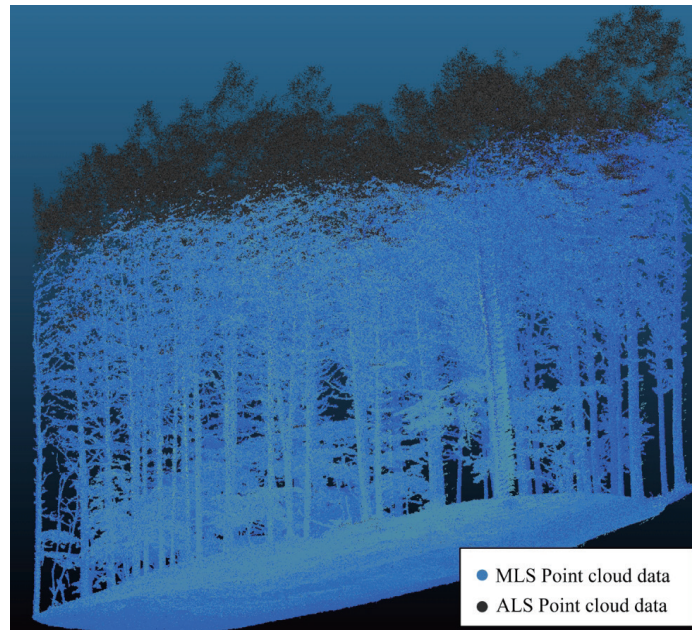


Fig. 5. (Color online) Merged PCD based on MLS and ALS PCD.

DBH and height (Fig. 5). Paris *et al.* and Dai *et al.* investigated LiDAR applications using merged MLS and ALS data.<sup>(20, 21)</sup> In this study, the merged PCD were obtained using both MLS and ALS. However, for high-density forests, only under-canopy PCD can be captured using ALS because of low light penetration to the ground surface. The results of this study show that integrated ALS and MLS overcame the problem of low light penetration in high-density forests.

### 3.2 Results of individual DBH estimation

Before estimating DBH, we evaluated the accuracy of the RANSAC algorithm as a function of the number of iterations. The estimated average RMSE of DBH was calculated as 1.14 cm for 10 iterations and monotonically decreased to 0.8 cm after 50 iterations. In addition, the RMSE decreased monotonically from 1.4 after 10 iterations to 0.8 cm after 40 iterations. Above 40 iterations, the fluctuation of average RMSE gradually decreased to below 0.1 cm. This means that increasing the number of iterations does not increase the accuracy of the RANSAC algorithm. On the basis of this result, the number of iterations used for DBH estimation was set to 50 when applying the circular fitting algorithms (Fig. 6).

The ground truth and DBH estimation algorithms, RCF, MEC, and EF, were compared to validate the LiDAR estimation. We used  $R^2$ , RMSE,  $t$ -test, and ANOVA to evaluate the accuracy of DBH estimation. The EF algorithm exhibited the lowest RMSE value and the highest  $R^2$  value among the three DBH estimation algorithms. The RMSE values estimated from the three algorithms were compared to determine the most suitable DBH estimation algorithm (Table 3, Fig. 7). The estimated  $R^2$  values of RCF, MEC, and EF were 0.99, 0.98, and 0.99, respectively. The largest gap between the estimated results and the ground truth data was found for MEC.



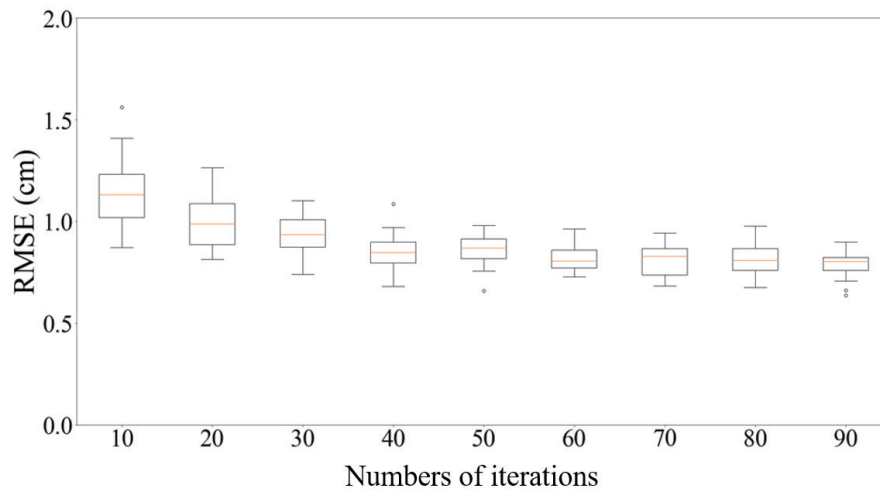


Fig. 6. (Color online) Box plot of RMSE distribution with different numbers of iterations.

Table 3

Results of DBH estimation using LiDAR and ground truth value (unit: cm).

Tree No.	Ground truth	Result of estimation			Bias		
		RCF	MEC	EF	RCF	MEC	EF
1	30	29.2	34.6	29.9	-0.8	4.6	-0.1
2	21.3	20.9	26.3	21.4	-0.4	5	0.1
3	28.5	27.8	34.5	29	-0.7	6	0.5
4	12.2	10.8	15.8	11.3	-1.4	3.6	-0.9
5	31.2	30.1	34	29.5	-1.1	2.8	-1.7
6	41	40.1	45.8	40.3	-0.9	4.8	-0.7
7	26.5	27.4	33	26.9	0.9	6.5	0.4
8	22.3	22.3	27.1	21.9	0	4.8	-0.4
9	29.5	28.7	34.5	29.3	-0.8	5	-0.2
10	35.8	36.1	42.1	35.4	0.3	6.3	-0.4
11	27.8	28.9	34.9	27.8	1.1	7.1	0
12	38.5	37.7	43.7	37.5	-0.8	5.2	-1
13	34	32	40	32.8	-2	6	-1.2
14	23	21.7	29.1	22.5	-1.3	6.1	-0.5
15	24.1	23.1	28.6	23.4	-1	4.5	-0.7
16	29.5	28.8	34.7	29	-0.7	5.2	-0.5
17	31.5	30.9	37.1	31.3	-0.6	5.6	-0.2
18	27	26.2	31.9	26.2	-0.8	4.9	-0.8
19	21.8	21.9	26.7	21.1	0.1	4.9	-0.7
20	21	21.1	25.6	20.2	0.1	4.6	-0.8
21	20.4	19.4	25.4	20	-1	5	-0.4
22	34.5	34.9	41.6	34.9	0.4	7.1	0.4
23	28.8	28.2	33.4	28	-0.6	4.6	-0.8
24	48	46.9	53.1	47.4	-1.1	5.1	-0.6
25	19.6	18.6	24.5	19	-1	4.9	-0.6
Mean	28.3	27.7	33.5	27.8			
SD	7.7	7.7	8.0	7.7			
RMSE	—	0.90	5.29	0.69			



Fig. 7. (Color online) Results of estimated individual tree DBH.

However, MEC overestimated DBH compared with the ground truth data. Among the circular fitting algorithms, EF exhibited the lowest error (Fig. 8). According to the *t*-test, the ground truth and DBH estimation algorithms gave significantly different results. However, the result of ANOVA for DBH estimation using LiDAR was not significantly different among the ground truth, RCF, and EF fitting. However, the MEC fitting algorithm showed a significant difference compared with the other methods ( $p > 0.05$ ) (Table 4).

In a previous study by Woo *et al.*, the minimum ellipse circle fitting algorithm showed the most accurate DBH estimation. In addition, the RMSE of the minimum ellipse circle showed the lowest volume estimation among four circular fitting algorithms.<sup>(9)</sup> Additionally, Bienert *et al.* investigated tree DBH using integrated MLS and TLS LiDAR systems. The results of their research indicated that the least-squares cylinder-fitting algorithm was the most accurate with an RMSE of 3.7 cm.<sup>(22)</sup> In the previous studies of comparing circular fitting applications for tree

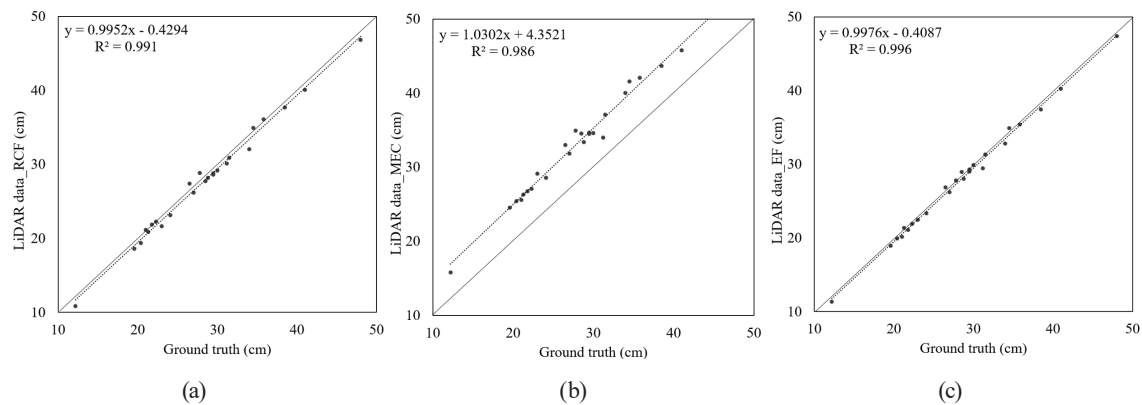


Fig. 8. (Color online) Scatter plots of DBH estimation (cm) from ground truth against estimation algorithm for (a) RCF, (b) MEC, and (c) EF.

Table 4

Statistical correlation based on ANOVA for DBH.

Algorithm	<i>df</i>	<i>F</i>	<i>p</i> -value	<i>F</i> critical value
Ground truth, RANSAC + circle fitting, EF	2	0.0388	0.9620	3.1239
Ground truth, RANSAC + circle fitting, EF, MEC	3	3.1922	0.0270	2.6994

DBH, different accuracies were obtained. Measurement accuracy may depend on the species or shape of the tree, as well as the method of data collection. In particular, our research indicated that the density of the PCD affects the estimated tree DBH because of overestimation. On the basis of this result, we have revealed that various circular fitting algorithms are required to accurately estimate the different shapes of individual trees.

### 3.3 Results of individual tree height estimations

The results indicated that the number of trees with PCD tree shapes of type A was 12 and type B was 10. However, only three trees were identified to be type C. In field measurements, the average tree height was measured to be 21.0 m and SD was estimated to be 2.7 m. However, the average tree height estimated using the CHM was 20.3 m with SD of 1.0 m (Table 5).

Tree height measurements using the CHM showed that types A and B were underestimated compared with the ground truth values. However, the tree height was overestimated using the CHM for type C. Additionally, the estimated RMSE was approximately 2.0 m for all types; the estimated RMSE values were calculated to be 1.9, 2.0, and 2.2 m for types A, B, and C, respectively. The most accurate tree height estimation was for type A trees. The *t*-test between the estimated height and the field-measured height showed no significant difference between the heights ( $p > 0.05$ ). The height was estimated less accurately for suppressed trees than for dominant trees (Fig. 9). This trend of less accuracy for suppressed trees was identified in the point extraction in the treetop detection from the overlapped PCD among the point clouds of surrounding dominant trees. Ullah *et al.* estimated tree height using the CHM based on ALS PCD<sup>(23)</sup> and estimated the overall RMSE to be 1.93 m. In addition, Peng *et al.* calculated the

Table 5  
Results of tree height estimation using LiDAR and ground truth values (unit: m).

Type	Tree No.	Ground truth	Result of estimation	Bias	
A	1	22.4	20.2	-2.2	
	2	17.9	19.1	1.2	
	12	22.7	20.4	-2.3	
	13	23.4	20.2	-3.2	
	14	18.0	18.8	0.8	
	15	20.9	20.3	-0.6	
	16	23.0	20.6	-2.4	
	17	23.7	21.1	-2.6	
	18	21.5	20.6	-0.9	
	20	18.5	20.2	1.7	
	22	21.4	20.9	-0.5	
	23	19.7	20.1	0.4	
		Mean	21.1	20.5	
		SD	2.1	1.1	
	$R^2$	—	0.579	—	
	RMSE	—	1.9		
B	4	19.5	19.4	-0.1	
	5	21.9	21.5	-0.4	
	6	23.9	21.7	-2.2	
	7	19.6	18.9	-0.7	
	8	21.8	20.8	-1.0	
	9	23.6	22.2	-1.4	
	10	23.5	20.1	-3.4	
	11	22.8	20.2	-2.6	
	21	18.3	19.0	0.7	
	24	24.8	21.0	-3.8	
		Mean	22.0	20.1	
		SD	2.2	0.7	
		$R^2$	—	0.596	—
		RMSE	—	2.0	
C	3	15.9	20.6	4.7	
	19	16.3	20.6	4.3	
	25	13.1	17.8	4.7	
		Mean	17.7	19.7	
		SD	2.7	1.6	
		$R^2$	—	0.990	—
	RMSE	—	2.2		
Total		Mean	21.0	20.3	
		SD	2.7	1.0	
		$R^2$	—	0.598	—
		RMSE	—	2.0	

RMSE of the estimated tree height to be 3.4 m.<sup>(24)</sup> The results of this study indicate that the integrated ALS and MLS PCD led to better performance in estimating tree height than that in previous studies on tree height estimation. The average tree height was estimated to be 21 m, with the height of trees having less than average height generally being underestimated and the height of trees with greater than average height generally being overestimated (Fig. 9). This

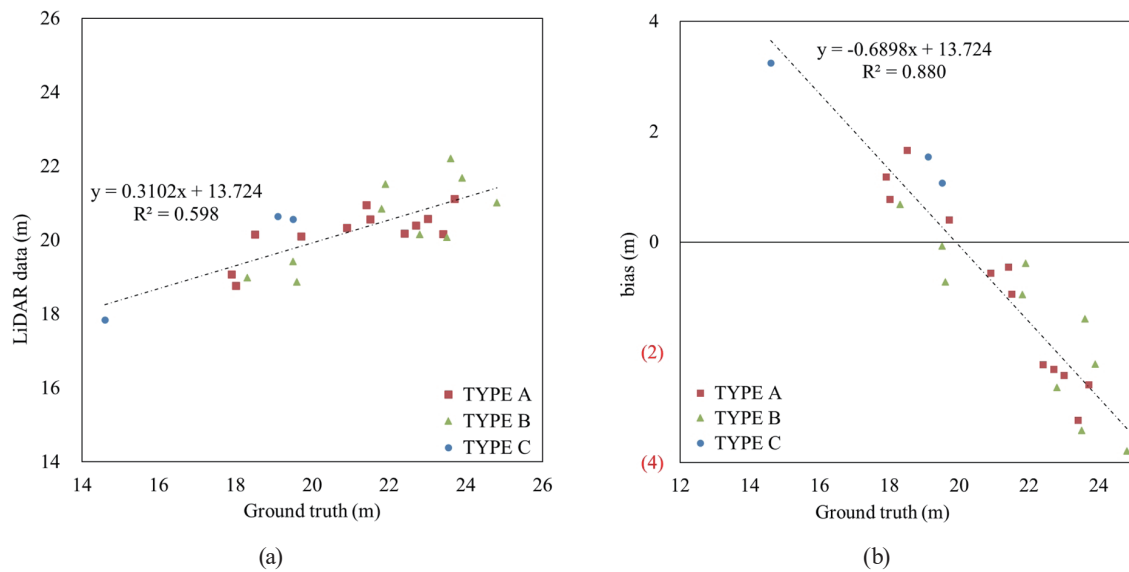


Fig. 9. (Color online) Scatter plots of ground truth height (m) and height estimated using LiDAR data. (a) Linear relationship between LiDAR estimation and ground truth data. (b) Bias variance against ground truth tree height.

result indicates that there are limitations in the effectiveness of segmenting the top portion of tree PCD for suppressed trees owing to overlap of dominant trees in a high-density forest structure. In addition, ALS is of limited use in capturing ground points of dominant trees owing to the dense forest structure. Because of the high density of forest structures, the application of LiDAR resulted in both the underestimation and overestimation of the tree height.<sup>(19,24,25)</sup>

#### 4. Conclusions

We investigated the applicability and limitations of using LiDAR applications to estimate individual tree DBH and height. We performed field measurements on 25 trees to validate the LiDAR estimation. The DBH estimation was the most accurate for EF, and the least-squares cylinder-fitting algorithm was the most accurate among the adopted circular fitting algorithms. Compared with previous circular fitting applications, integrated ALS and MLS performed better in estimating tree DBH. In addition, most circular fitting algorithms show different accuracies of DBH estimation depending on the data collection method and the shape of individual trees. Our research indicates that the PCD density impacts tree DBH estimation.

The tree height estimated using the CHM was compared with the ground truth, and  $R^2$  and RMSE of the height were 0.60 and 2.0 m, respectively. In this study, we established the applicability and limitations of using LiDAR systems to conduct forest inventory assessments. In addition, the trend of lower accuracy for suppressed trees was identified in PCD extraction for the detection of treetops from the overlapped PCD among the surrounding dominant trees. This result indicated that the case of suppressed trees is limited in the estimation of tree height using PCD owing to overlap by dominant trees in high-density forest structures. In addition, in a dominant trees plot with a high-density forest structure, it is difficult to capture ground points

owing to the high density of forest crowns. Because of the highly dense forest structure, LiDAR sometimes underestimates or overestimates tree heights.

There are many efforts to estimate forest structure using LiDAR systems. However, to be able to apply LiDAR to the forest industry in the future, it is necessary to set the tree position within the LiDAR data without reference data. Meanwhile, research is being conducted to set tree locations using various analysis tools, such as segmentation and cluster analysis.<sup>(8,26)</sup> Linking the results of such studies and the present study will be valuable in the application of LiDAR in the forest industry.

### Acknowledgments

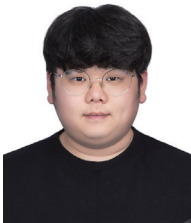
This study was carried out with the support of the R&D Program for Forest Science Technology (Project No. 2021359B10-2223-BD01) provided by the Korea Forest Service (Korea Forestry Promotion Institute).

### References

- 1 H. M. Hoganson and N. G. Meyer: *Curr. For. Rep.* **1** (2015). <https://doi.org/10.1007/s40725-015-0004-x>
- 2 J. C. White, N. C. Coops, M. A. Wulder, M. Vastaranta, T. Hilker, and P. Tompalski: *Can. J. Remote Sens.* **42** (2016) 5. <https://doi.org/10.1080/07038992.2016.1207484>
- 3 P. Surový and K. Kuželka: *Forests* **10** (2019) 3. <https://doi.org/10.3390/f10030273>
- 4 K. Zhao, S. Popescu, and R. Nelson: *Remote Sens. Environ.* **113** (2009) 1. <https://doi.org/10.1016/j.rse.2008.09.009>
- 5 J. R. Ben-Arie, G. J. Hay, R. P. Powers, G. Castilla, and B. St-Onge: *Comput. Geosci.* **35** (2009) 9. <https://doi.org/10.1016/j.cageo.2009.02.003>
- 6 S. C. Popescu, R. H. Wynne, and R. F. Nelson: *Can. J. Remote Sens.* **29** (2003) 5. <https://doi.org/10.5589/m03-027>
- 7 J. J. Donager, A. J. Sánchez Meador, and R. C. Blackburn: *Remote Sens.* **13** (2021) 12. <https://doi.org/10.3390/rs13122297>
- 8 L. Liu, A. Zhang, S. Xiao, S. Hu, N. He, H. Pang, X. Zhang, and S. Yang: *IEEE Access* **9** (2021) 24314. <https://doi.org/10.1109/ACCESS.2021.3056877>
- 9 H. Woo, I. Kim, and B. Choi: *Sens. Mater.* **33** (2021) 11. <https://doi.org/10.18494/SAM.2021.3605>
- 10 J. R. Kellner, J. Armston, M. Birrer, K. C. Cushman, L. Duncanson, C. Eck, C. Fallegger, B. Imbach, K. Král, and M. Krůček: *Surv. Geophys.* **40** (2019) 4. <https://doi.org/10.1007/s10712-019-09529-9>
- 11 A. P. Dalla Corte, F. E. Rex, Almeida, Danilo Roberti Alves de, C. R. Sanquetta, C. A. Silva, M. M. Moura, B. Wilkinson, A. M. A. Zambrano, Cunha Neto, Ernandes M da, and H. F. Veras: *Remote Sens.* **12** (2020) 5. <https://doi.org/10.3390/rs12050863>
- 12 L. Jurjević, M. Gašparović, X. Liang, and I. Balenović: *Remote Sens.* **13** (2021) 11. <https://doi.org/10.3390/rs13112063>
- 13 T. Kersten, J. Wolf, and M. Lindstaedt: *ISPRS Ann. Photogramm. Remote Sens. Spatial Inf. Sci.* **43** (2022) 339. <https://doi.org/10.5194/isprs-archives-XLIII-B1-2022-339-2022>
- 14 B. Wilkinson, H. A. Lassiter, A. Abd-Elrahman, R. R. Carthy, P. Ifju, E. Broadbent, and N. Grimes: *Remote Sens.* **11** (2019) 24. <https://doi.org/10.3390/rs11243019>
- 15 P. J. Besl and N. D. McKay: *IEEE Trans. Pattern. Anal. Mach. Intell.* **14** (1992) 2. <https://doi.org/10.1117/12.57955>
- 16 K. Kuželka, M. Slavík, and P. Surový: *Remote Sens.* **12** (2020) 8. <https://doi.org/10.3390/rs12081236>
- 17 H. Huang, Z. Li, P. Gong, X. Cheng, N. Clinton, C. Cao, W. Ni, and L. Wang: *Photogramm. Eng. Remote Sens.* **9** (2011) 219. <https://doi.org/10.14358/PERS.77.3.219>
- 18 X. Liang, J. Hyypä, H. Kaartinen, M. Lehtomäki, J. Pyörälä, N. Pfeifer, M. Holopainen, G. Brolly, P. Francesco, and J. Hackenberg: *ISPRS J. Photogramm. Remote Sens.* **144** (2018) 137. <https://doi.org/10.1016/j.isprsjprs.2018.06.021>
- 19 M. Mielczarek, K. Stereńczak, and A. Khosravipour: *Int. J. Appl. Earth Obs. Geoinf.* **71** (2018) 132. <https://doi.org/10.1016/j.jag.2018.05.002>

- 20 C. Paris, D. Kelbe, J. Van Aardt, and L. Bruzzone: IEEE Trans. Geosci. Remote Sens. **55** (2017) 7. <https://doi.org/10.1109/TGRS.2017.2675963>
- 21 W. Dai, B. Yang, X. Liang, Z. Dong, R. Huang, Y. Wang, and W. Li: ISPRS J. Photogramm. Remote Sens. **156** (2019) 94. <https://doi.org/10.1016/j.isprsjprs.2019.08.008>
- 22 A. Bienert, L. Georgi, M. Kunz, H. Maas, and G. Von Oheimb: Forests **9** (2018) 7. <https://doi.org/10.3390/f9070395>
- 23 S. Ullah, P. Adler, M. Dees, P. Datta, H. Weinacker, and B. Koch: IForest **10** (2017) 1. <https://doi.org/10.3832/ifor2077-009>
- 24 X. Peng, A. Zhao, Y. Chen, Q. Chen, and H. Liu: Forests **12** (2021) 3. <https://doi.org/10.3390/f12030328>
- 25 D. L. Gaveau and R. A. Hill: Can. J. Remote Sens. **29** (2003) 5. <https://doi.org/10.5589/m03-023>
- 26 H. Fu, H. Li, Y. Dong, F. Xu, and F. Chen: Forests **13** (2022) 4. <https://doi.org/10.3390/f13040566>

## About the Authors



**Yongkyu Lee** received his B.S. and M.S. degrees from Kangwon National University, Korea, in 2019 and 2021, respectively, and is currently studying for a Ph.D. degree. His research interests include forest spatial analysis using GIS and RS. ([kong445566@kangwon.ac.kr](mailto:kong445566@kangwon.ac.kr))



**Heesung Woo** received his B.S. degree from Kangwon National University, South Korea, in 2011, his first and second M.S. degrees from Kangwon National University, South Korea, in 2013 and Humboldt State University, CA, USA, in 2015, respectively, and his Ph.D. degree from the University of Tasmania, Australia, in 2020. From 2019 to 2020, he was a research professor at Kyungpook National University, South Korea. Since 2021, he has been a research professor at Kangwon National University. His research interests are in precision forestry, robotics, sensors, and data analysis in forest management. ([whs1608@gmail.com](mailto:whs1608@gmail.com))



**Jung-Soo Lee** received his B.S. degree from Kangwon National University, Republic of Korea, in 1998 and his M.S. and Ph.D. degrees from Tokyo University, Japan, in 2000 and 2003, respectively. Since 2006, he has been a professor at Kangwon National University. His research interests include GIS, and remote sensing related to forest management. ([jslee72@kangwon.ac.kr](mailto:jslee72@kangwon.ac.kr))